materials

MDPI

Article

CO_2 Adsorption over 3*d* Transition-Metal Nanoclusters Supported on Pyridinic N_3-Doped Graphene: A DFT Investigation

Fernando Montejo-Alvaro [1,†], Jesus A. Martínez-Espinosa [2,†], Hugo Rojas-Chávez [3], Diana C. Navarro-Ibarra [1], Heriberto Cruz-Martínez [1,*] and Dora I. Medina [2,*]

1 Tecnológico Nacional de México, Instituto Tecnológico del Valle de Etla, Abasolo S/N, Barrio del Agua Buena, Santiago Suchilquitongo, Oaxaca 68230, Mexico
2 Tecnologico de Monterrey, School of Engineering and Sciences, Atizapán de Zaragoza, Estado de México 52926, Mexico
3 Tecnológico Nacional de México, Instituto Tecnológico de Tláhuac II, Camino Real 625, Col. Jardines del Llano, San Juan Ixtayopan, Alcaldía Tláhuac, Ciudad de México 13550, Mexico
* Correspondence: heri1234@hotmail.com (H.C.-M.); dora.medina@tec.mx (D.I.M.)
† These authors contributed equally to this work.

Abstract: CO_2 adsorption on bare 3*d* transition-metal nanoclusters and 3*d* transition-metal nanoclusters supported on pyridinic N_3-doped graphene (PNG) was investigated by employing the density functional theory. First, the interaction of Co_{13} and Cu_{13} with PNG was analyzed by spin densities, interaction energies, charge transfers, and HUMO-LUMO gaps. According to the interaction energies, the Co_{13} nanocluster was adsorbed more efficiently than Cu_{13} on the PNG. The charge transfer indicated that the Co_{13} nanocluster donated more charges to the PNG nanoflake than the Cu_{13} nanocluster. The HUMO-LUMO gap calculations showed that the PNG improved the chemical reactivity of both Co_{13} and Cu_{13} nanoclusters. When the CO_2 was adsorbed on the bare 3*d* transition-metal nanoclusters and 3*d* transition-metal nanoclusters supported on the PNG, it experienced a bond elongation and angle bending in both systems. In addition, the charge transfer from the nanoclusters to the CO_2 molecule was observed. This study proved that Co_{13}/PNG and Cu_{13}/PNG composites are adequate candidates for CO_2 adsorption and activation.

Keywords: CO_2 adsorption and activation; HUMO-LUMO gap; charge transfer; stability

Citation: Montejo-Alvaro, F.; Martínez-Espinosa, J.A.; Rojas-Chávez, H.; Navarro-Ibarra, D.C.; Cruz-Martínez, H.; Medina, D.I. CO_2 Adsorption over 3*d* Transition-Metal Nanoclusters Supported on Pyridinic N_3-Doped Graphene: A DFT Investigation. *Materials* **2022**, *15*, 6136. https://doi.org/10.3390/ma15176136

Academic Editor: George Alexandru Nemnes

Received: 18 July 2022
Accepted: 30 August 2022
Published: 4 September 2022

1. Introduction

Due to environmental changes such as rising global temperatures, sea levels, and melting of the polar ice caps, concerns are accumulating around the presence of CO_2 in the atmosphere [1]. Furthermore, population growth and rapid industrialization have escalated the release of CO_2 into the atmosphere [2]. In addition, energy requirements for human activities (anthropogenic) have contributed substantially to net CO_2 emissions [3]. In fact, anthropogenic CO_2 emissions have dramatically increased from 27 Gt in 1970 to 49 Gt in 2010 [4]. As a result, many governments have signed the Kyoto Protocol of the United Nations Framework Convention on Climate Change as a precautionary measure to mitigate climate change [5].

Additionally, several technological processes have been implemented to curb CO_2 accumulation by implementing techniques such as the CO_2 capturing and sequestration process [6], CO_2 capturing and utilization processes [7], and CO_2 conversion [8,9]. Yet, the enormous dissociation energy of CO_2 resulting from its molecular stability limits the feasibility of the latter process [10]. Moreover, challenges in developing suitable catalysts in terms of efficiency and selectivity still stand unresolved [11]. That notwithstanding, strides in this area continually seek to find more efficient catalysts that diminish process energy requirements and show high selectivity and stability to CO_2 reduction reactions.

In this regard, a wide variety of catalysts have been studied: primarily, current studies have been centered on nanoclusters, since they exhibit superior catalytic activity with respect to bulk materials handling, enabled by their specific surface area, electronic, optical, magnetic, and mechanical properties, which are strongly associated with their shape, size, and composition [12]. Thus, 3*d* transition-metal nanoclusters have gained considerable attention since they have demonstrated remarkable performance in CO_2 reduction. For instance, the removal and conversion of CO_2 into liquid fuels using amorphous Cu nanoparticles showed an excellent catalytic activity and selectivity [13]. In another study, Li and colleagues studied the CO_2 reduction over Ni-based electrocatalysts with sizes ranging from a few atoms to over 100 nm. Their results imply that CO_2 reduction and selectivity performance vary according to the size of Ni nanoparticles [14]. Furthermore, another study used Co nanoparticles ranging from 10 to 50 nm prepared for CO_2 methanation and ethanol reforming, demonstrating the nanoparticles' significant activity in the process [15].

Though the catalytic activities of nanoclusters are acclaimed, they tend to agglomerate, resulting in a decline in activity and stability [16–18]. Therefore, addressing this issue requires the use of high-surface-area nanomaterials to anchor nanoparticles to promote stability and activation. One of the most eminent nanomaterials in this respect is graphene which exhibits high mechanical, thermal, and electrical properties [19–21]. Nonetheless, graphene often necessitates modifications such as doping, functionalization, or the presence of defects on its surface. These adjustments are intended to overcome the low chemical activity of graphene [21,22]. Among the different modifications made to graphene, the pyridinic N_3-doped graphene (PNG) has acquired great importance since it substantially modifies the structural and electronic properties of the pristine graphene. Furthermore, studies based on density functional theory (DFT) have proved that the stability and reactivity of metal nanoclusters were enhanced using PNG layers as support [23–25].

Moreover, using 3*d* transition-metal nanoclusters supported on PNG for CO_2 reduction has been studied experimentally. For example, Dongare and collaborators investigated electrochemical CO_2 reduction using N-doped graphene-supported Cu nanoparticles. The presence of pyridinic, pyrrolic, and graphitic N were confirmed using X-ray photoelectron spectroscopy (XPS). Furthermore, the high PNG content signified good selectivity toward CO_2 reduction. In the end, the N-doped graphene/Cu nanoparticles composite enhanced the activity and selectivity in CO_2 reduction [26]. Likewise, the incorporation of MnO nanoparticles into an N-doped graphene aerogel for CO_2-to-CO electrochemical reduction was studied. According to XPS spectra, it was found that the primary N species was the pyridinic type. Their results suggest that CO_2-to-CO electrochemical reduction was enhanced by the synergistic effect of the MnO nanoparticles and the N-doped aerogels [27]. Thus, these studies emphasize the central role of N-doped graphene in CO_2 reduction. However, there are no theoretical studies that analyze the effect of the PNG support on the stability and catalytic activity of 3*d* transition-metal clusters toward CO_2 at the molecular level. Therefore, in this work, CO_2 adsorption and activation on bare 3*d* transition-metal nanoclusters and 3*d* transition-metal supported nanoclusters were investigated using DFT calculations, since their adsorption and activation on surfaces are key steps in the CO_2 conversion reaction [28]. To analyze the CO_2 interaction on both bare nanoclusters and nanoclusters supported on PNG, the CO_2 adsorption energy, CO_2 bond elongation, CO_2 bending angle, and charge transfer are calculated since these are indicators of effective CO_2 dissociation [29–32].

2. Materials and Methods

To obtain the most stable CO_2 adsorption on both the bare nanoclusters and nanoclusters supported on PNG graphene, nine initial structures were considered. All initial structures were optimized using the auxiliary density functional theory (ADFT) method implemented in the deMon2k 4.3.8 software [33]. The ADFT is a reliable and efficient alternative to the conventional DFT approach that allows calculations of large complex systems with less computational effort. The revised Perdew–Burke–Ernzerhof (revPBE)

functional was used as the exchange–correlation functional [34]. For the Co, H, C, O, and N atoms, a double-zeta valence plus polarization basis set optimized for generalized gradient approximation (GGA) functionals (DZVP-GGA) was employed [35], and a triple-zeta valence plus polarization basis set optimized for GGA functionals (TZVP-GGA) was used for the Cu atoms [35]. The most stable structures obtained with the ADFT method were reoptimized with the conventional DFT method using the Orca 5.0 software [36]. All DFT calculations were performed using revPBE [34]. The Ahlrichs basis set def2-SVP was used for the C, N, O, and H atoms, and def2-TZVP was used for the Co and Cu atoms [37]. The energy change = 5×10^{-6} Eh, max. gradient = 3×10^{-4} Eh/Bohr, RMS gradient = 1×10^{-4} Eh/Bohr, max. displacement = 4×10^{-3} Bohr, and RMS displacement = 2×10^{-3} Bohr were the convergence criteria used for geometry optimization.

The icosahedral Co_{13} and Cu_{13} nanoclusters (Figure 1a) and the graphene model (Figure 1b) used in this work are reported in Figure 1.

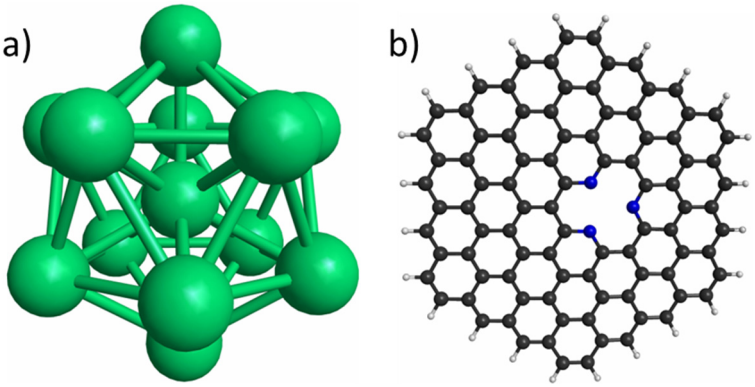

Figure 1. (**a**) Icosahedral metal nanoclusters with 13 atoms; (**b**) Pyridinic N_3-doped graphene. Green, black, white, and blue spheres represent metal (Co or Cu), C, H, and N atoms, respectively.

The CO_2 adsorption energies (E_{ads}) on isolated nanoclusters and nanoclusters supported on PNG were calculated using the basis set superposition error (BSSE) [38]. Moreover, the atom-pairwise (atom-triplewise) dispersion (D3) correction was used for the RevPBE functional using optimized parameters by Grimme et al. [39]. Finally, to analyze the molecular interactions of the Co_{13} and Cu_{13} nanoclusters supported on PNG and the CO_2 adsorption over bare nanoclusters and nanoclusters supported on PNG, the quantum theory of atoms in molecules implemented in the Multiwfn program was used [40].

3. Results

3.1. Properties of Co_{13}, Cu_{13}, Co_{13}/PNG, and Cu_{13}/PNG

First, comparison of the spin multiplicities of bare nanoclusters and nanoclusters supported on the PNG was made. The Co_{13} and Cu_{13} nanoclusters possess spin multiplicity values of 32 and 6, respectively, which agree with previous results reported for the Co_{13} [41] and Cu_{13} [42] nanoclusters. The optimized Co_{13} and Cu_{13} nanoclusters supported on PNG are illustrated in Figure 2. When the Co_{13} and Cu_{13} nanoclusters are supported on PNG, a decrement in spin multiplicity was observed in the supported nanoclusters compared to the bare nanoclusters. The Co_{13}/PNG composite ended with a spin multiplicity value of 27, whereas the Cu_{13}/PNG composite was singlet. The spin multiplicity diminution observed in both systems is ascribed to the stabilizing effect of the PNG. This is also consistent with data reported in literature. For instance, for the Pd- and Pt-based nanoclusters supported on the PNG nanoflake, the latter lead to a magnetic-moment decrement in most of the systems; such behavior was associated with the charge transferred from the nanoclusters to the PNG nanoflake [23,24].

Spin densities, interaction energies (E_{int}), and charge transfers were calculated to better understand the interaction between the nanoclusters and PNG support. In Figure 3 the spin density of the Co_{13} nanocluster supported on the PNG is illustrated, since it is an open-shell

system, and the spin density of the Co_{13} nanocluster is also computed for comparison. As can be seen in Figure 3a, for the Co nanocluster, there is a homogeneous spin density distribution over the Co atoms. When the Co nanocluster is supported on the PNG, the spin density is distributed mostly on the Co atoms and little on the N atoms (Figure 3b).

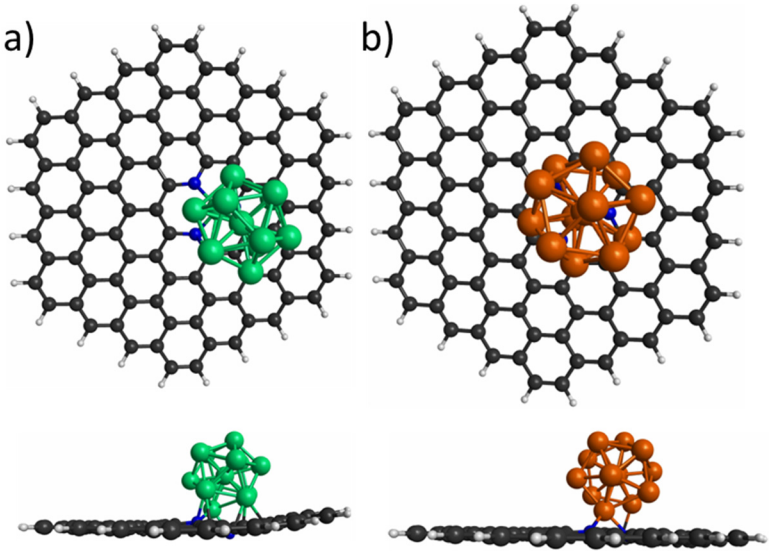

Figure 2. Top and side views of the most stable interaction of (**a**) Co_{13} and (**b**) Cu_{13} nanocluster deposited on pyridinic N_3-doped graphene. Green, orange, black, white, and blue spheres represent Co, Cu, C, H, and N atoms, respectively.

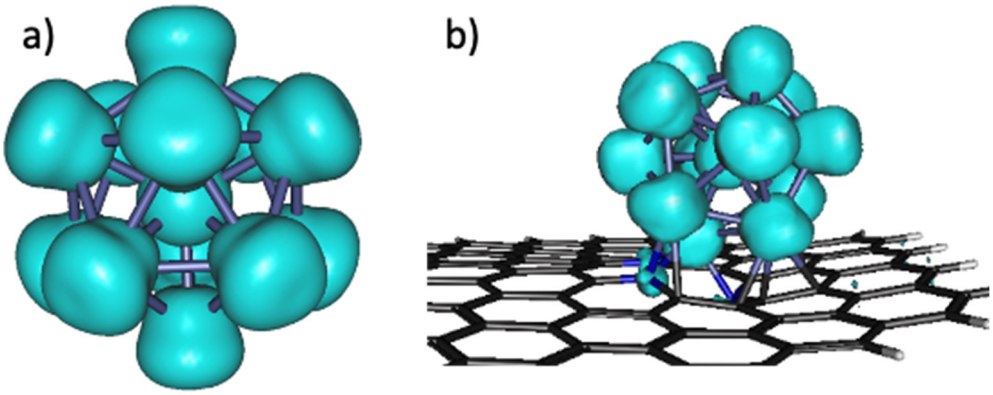

Figure 3. Spin density distributions of the systems: (**a**) Co_{13} nanocluster and (**b**) Co_{13}/PNG composite.

The E_{int} calculated for the Co_{13} and Cu_{13} nanoclusters supported on PNG are −5.69 eV and −4.72 eV, respectively. It should be noted that both values are substantially higher than those reported in previous findings for the Co_{13} [43,44] and Cu_{13} [45,46] nanoclusters supported on pristine graphene. Therefore, PNG has a more substantial stabilizing effect over the Co_{13} and Cu_{13} nanoclusters compared to pristine graphene. The interaction between the Co_{13} and Cu_{13} nanoclusters with PNG was further investigated by Bader charge transfer. The charge transfer between the Co_{13} and Cu_{13} nanoclusters and the PNG is reported in Table 1. The results suggest that both nanoclusters yielded charge to the PNG since both ended with a total positive charge. The large electronegativity of N and the electronegativity difference of Co and Cu atoms are the principal driving force for the charge transfer. Furthermore, the highest occupied molecular orbital (HOMO) and lowest unoccupied molecular orbital (LUMO) gap was computed for the bare Co_{13} and Cu_{13} nanoclusters and the Co_{13}/PNG and Cu_{13}/PNG composites, Table 1. The Co_{13} and Cu_{13} nanoclusters show HOMO-LUMO gaps of 0.52 and 0.67 eV, respectively, which imply that the Co_{13} can be more reactive than the Cu_{13} nanocluster as it has been documented

that a low HOMO-LUMO gap is associated with high chemical reactivity [45,47,48]. The HOMO-LUMO gaps of the Co_{13}/PNG (0.26 eV) and Cu_{13}/PNG (0.21 eV) were lower than that for the bare nanoclusters. Therefore, it is assumed that the presence of the PNG increased the chemical reactivity of the nanoclusters.

Table 1. Charge transfers and HOMO-LOMO gaps for Co_{13}, Cu_{13}, Co_{13}/PNG, and Cu_{13}/PNG. The positive values indicate charge transfers from the nanoclusters to the PNG structure.

Systems	HOMO-LOMO Gap (eV)	Charge Transfer (*e*)
Co_{13}	0.52	-
Cu_{13}	0.67	-
Co_{13}/PNG	0.26	+1.40
Cu_{13}/PNG	0.21	+0.78

3.2. CO_2 Adsorption on Co_{13} and Cu_{13} Nanoclusters

Several modes of CO_2 adsorption on both the bare nanoclusters and nanoclusters supported on PNG were investigated. First, the CO_2 molecule was placed over different facets of the Co_{13} and Cu_{13} nanoclusters to identify the most optimal adsorption modes. Due to the high symmetry of the icosahedral Co_{13} and Cu_{13} nanoclusters, only nine adsorption modes were considered (Figure 4). Specific parameters were considered to evaluate the CO_2 adsorption on the Co_{13} and Cu_{13} nanoclusters, such as the E_{ads}, the average bond length, the bending angle of the CO_2 molecule, and the charge transfer from the nanoclusters to the CO_2 molecule. These parameters were calculated over the most stable structures of CO_2 adsorption on nanoclusters and nanoclusters supported on PNG.

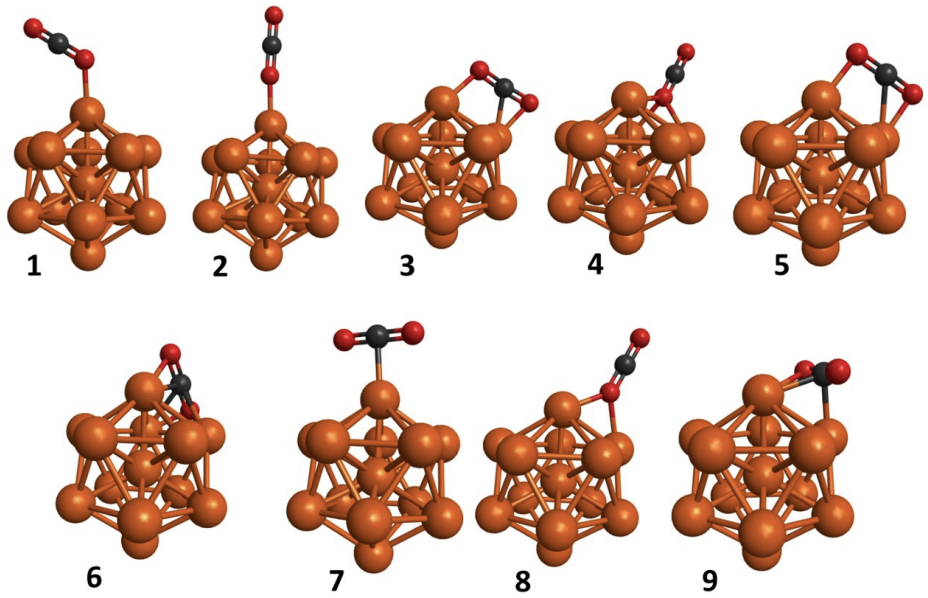

Figure 4. CO_2 adsorption modes on nanoclusters.

The most stable model of CO_2 adsorption on the Co_{13} and Cu_{13} nanocluster is depicted in Figures 5a and 5b, respectively. The results show that CO_2 bends when it is adsorbed on the Co_{13} and Cu_{13} nanoclusters. Although the CO_2 interaction on the Co_{13} nanocluster is consistent with the findings of other works [30], the interaction of CO_2 and Cu_{13} differs from the one reported in previous studies, because it was reported that CO_2 remained linear once adsorbed and only interacted with one Cu atom [30]. However, this distinct interaction might be attributed to the fact that they used nonicosahedral Cu_{13} nanoclusters.

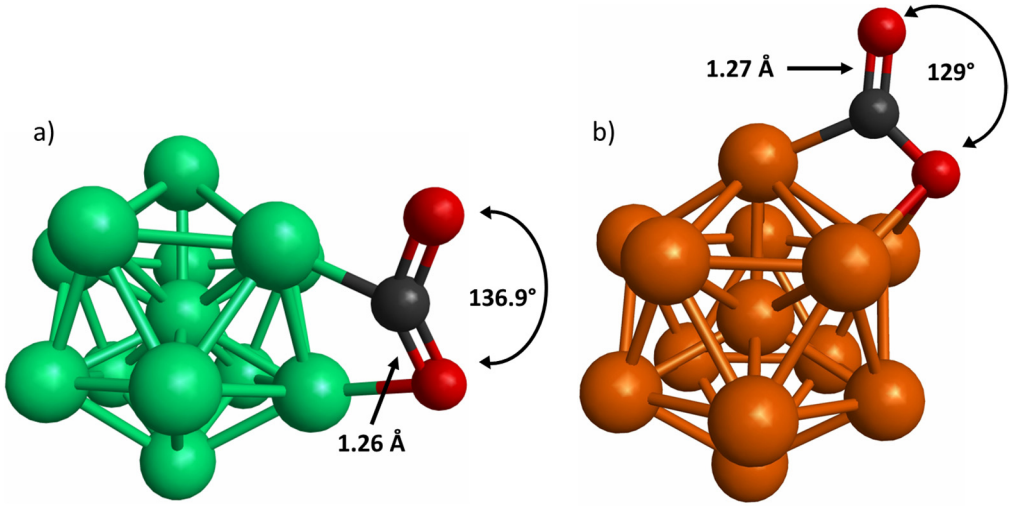

Figure 5. CO_2 adsorbed on (**a**) Co_{13} and (**b**) Cu_{13} nanoclusters. The average bond length (Å) and angle bending (°) of CO_2 molecule is depicted. Green, orange, black, and red spheres represent Co, Cu, C, and O atoms, respectively.

To estimate the interaction between the CO_2 molecule and the 3*d* transition-metal nanoclusters, the E_{ads} were calculated. In the case of the CO_2 adsorbed on the Co_{13} nanocluster, the E_{ads} was −0.94 eV. This value is like those reported in the literature [30,49]. The E_{ads} calculated for CO_2 on the Cu_{13} nanocluster was −0.18 eV, which agrees with the data reported in literature [30,49]. In addition, an average bond elongation of the CO_2 was observed when it was adsorbed on the Co_{13} nanocluster. Regarding the bending angle, there was a pronounced curving with a reduction of 23.94% with respect to the isolated CO_2 molecule. These parameters are comparable to those reported in previous works [30]. Concerning the average bond length and bending angle of the CO_2 molecule adsorbed on the Cu_{13} nanocluster. As in the CO_2 adsorbed on the Co_{13} nanocluster, an average bond elongation was observed. On the other hand, the bending angle underwent a considerable contraction of 28.34%. Nevertheless, these parameters do not concur with the values reported in earlier findings. In fact, Ocampo-Restrepo did not report this kind of modification in either the average bond length or bending angle of the CO_2 molecule [30].

3.3. CO_2 Adsorption on Co_{13} and Cu_{13} Nanoclusters Supported on PNG

To investigate the CO_2 adsorption on Co_{13}/PNG and Cu_{13}/PNG composites, we analyzed various adsorption modes described in the preceding section. Again, the E_{ads}, the average bond length, and the bending angle were determined to evaluate the CO_2 adsorption. The most optimal adsorption mode for Co_{13}/PNG and Cu_{13}/PNG composites is depicted in Figures 6a and 6b, respectively. For both composites, the CO_2 preferred to be adsorbed in a bent way. Subsequently, the E_{ads} of CO_2 on the Co_{13}/PNG and Cu_{13}/PNG composites was calculated. The results showed that the CO_2 adsorbs more intensely on the Co_{13}/PNG composite with a value of −0.92 eV, whereas the E_{ads} of CO_2 on the Cu_{13}/PNG composite was only −0.33 eV. As in the CO_2 adsorbed on bare clusters, an average bond elongation of CO_2 was observed when it was adsorbed on nanoclusters supported on PNG (Figure 6). Moreover, the CO_2 bending angle underwent a considerable contraction when it was adsorbed on Co_{13} (24.72%) and Cu_{13} (22.83%) supported on PNG.

3.4. Bonding Analysis of the CO_2 Interaction on Nanoclusters and Nanoclusters Supported on PNG

Table 2 shows the CO_2 charge transference when is adsorbed on Co_{13}, Cu_{13}, Co_{13}/PNG, and Cu_{13}/PNG. The total charge of the CO_2 molecule resulted in negative values for all systems, which indicates that the CO_2 molecule gained a charge after the adsorption. For instance, the CO_2 adsorption on the Co_{13} nanocluster enabled the CO_2 to gain a

charge of −0.74 *e*, indicating that the charge is transferred from the nanocluster to the CO_2 molecule. It was reported that the transfer plays a significant role in the activation of the CO_2 molecule [32,49].

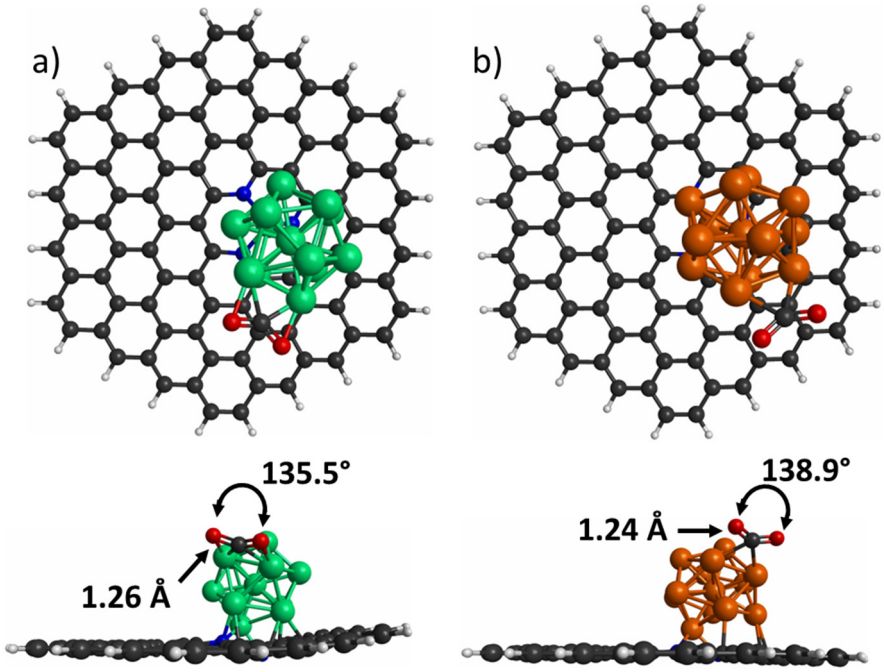

Figure 6. CO_2 adsorption on (**a**) Co_{13}/PNG and (**b**) Cu_{13}/PNG. The bond length (Å) and angle bending (°) of CO_2 molecule is depicted. Green, orange, black, white, blue, and red spheres represent Co, Cu, C, H, N, and O atoms, respectively.

Table 2. Charge transfer from Co_{13}, Cu_{13}, Co_{13}/PNG, and Cu_{13}/PNG to CO_2 molecule. The negative values indicate charge transfers from the nanoclusters and nanoclusters/PNG to the CO_2 molecule.

Systems	Charge Transfer toward CO_2 (*e*)
Co_{13}	−0.74
Cu_{13}	−0.78
Co_{13}/PNG	−0.75
Cu_{13}/PNG	−0.67

The electron localization function (ELF) was used to analyze the type of bond formed by the CO_2 interaction on free nanoclusters and nanoclusters supported on PNG. ELF analysis is widely used to understand the nature of chemical bonds, which allows for differentiating covalent bonds and lone pairs (ELF = 1), as well as ionic bonds, hydrogen bonds, and van der Waals interactions (ELF = 0). Figure 7 shows the ELF plots for the CO_2 adsorbed on nanoclusters and nanoclusters supported on PNG. As can be observed, the red region between the C atoms and the metal atom has ELF values of 0.8 and 0.9 for the C-Co (Figure 7a) and C-Cu bonds (Figure 7b), respectively. The high ELF value indicates a high charge transfer from the Cu_{13} to the CO_2 molecules, in accordance with the total charge calculated (see Table 2). For the CO_2 absorbed on the nanocluster/PNG, the ELF value is ~0.85 when the CO_2 is absorbed on the Co_{13}/PNG composite and ~0.8 when the CO_2 is absorbed on the Cu_{13}/PNG composite, suggesting a lower charge transfer from the metal cluster to the CO_2 molecule (see Figure 7c,d). For the CO_2 adsorption on Co_{13} and on Co_{13}/PNG, a red region between the C and Co is observed, suggesting a bonding C-Co. Meanwhile, for CO_2 on Cu_{13} a uniform red region is observed between C and a Cu. However, when CO_2 is adsorbed on Cu_{13}/PNG a semicircular region appears between C and two Cu atoms (see Figure 7d), suggesting that C is bonded with two Cu atoms.

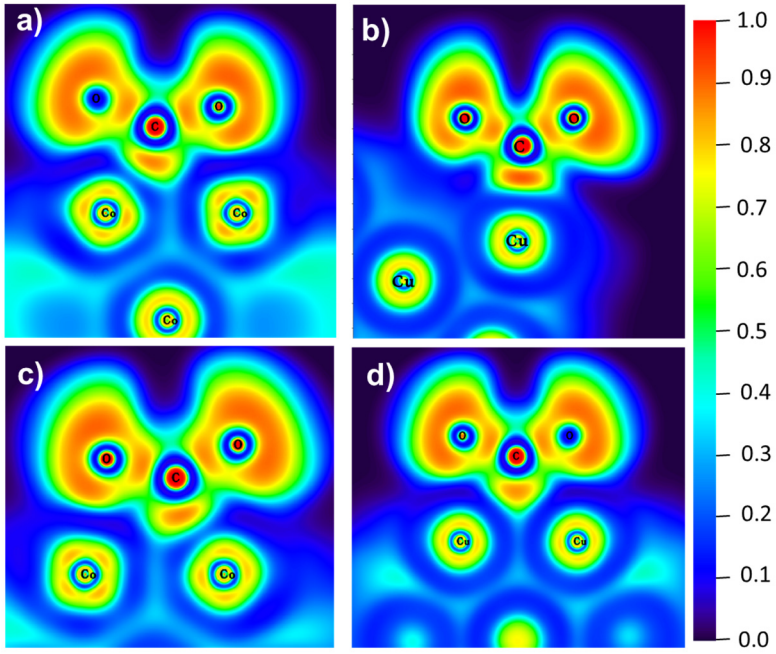

Figure 7. Electron localization function contours for: (**a**) CO_2 adsorption on Co_{13}, (**b**) CO_2 adsorption on Cu_{13}, (**c**) CO_2 adsorption on CO_{13}/PNG, and (**d**) CO_2 adsorption on Cu_{13}/PNG.

4. Conclusions

The CO_2 adsorption on bare 3*d* transition-metal nanoclusters and 3*d* transition-metal nanoclusters supported on the PNG was investigated using the ADFT. First, the interaction between Co_{13} and Cu_{13} nanoclusters with PNG was studied by spin densities, interaction energies, charge transfers, and HUMO-LUMO gaps. The results revealed that the PNG enhanced the stability and chemical reactivity of the 3*d* transition-metal nanoclusters. Subsequently, the CO_2 was adsorbed on bare 3*d* transition-metal nanoclusters, and 3*d* transition-metal nanoclusters supported PNG. Numerous indicators such as bond elongation, angle bending, and charge transfer were used to characterize the CO_2 interaction on these systems. In terms of bond elongation, bare nanoclusters and nanoclusters supported on PNG induced a CO_2 bond elongation. In addition, the CO_2 molecule experienced a bending angle when it was adsorbed on bare nanoclusters and nanoclusters supported on PNG. Charge transfer analysis revealed that the CO_2 gained charge when it was adsorbed on 3*d* transition-metal nanoclusters and 3*d* transition-metal nanoclusters supported on PNG nanosheet. Although the nanoclusters and nanoclusters supported on PNG exhibited similar reactivity towards CO_2, nanoclusters supported on PNG have the advantage of the support material providing excellent stability to the nanoclusters; therefore, they will not present agglomeration problems.

Author Contributions: Conceptualization, F.M.-A., J.A.M.-E., H.C.-M. and D.I.M.; methodology, F.M.-A., J.A.M.-E., H.R.-C., D.C.N.-I. and D.I.M.; formal analysis, F.M.-A., J.A.M.-E., H.R.-C., D.C.N.-I., H.C.-M. and D.I.M.; investigation, F.M.-A., J.A.M.-E. and H.R.-C.; writing—original draft preparation, F.M.-A., J.A.M.-E., H.R.-C., H.C.-M. and D.I.M.; writing—review and editing, H.C.-M. and D.I.M.; funding acquisition, F.M.-A., H.C.-M. and D.I.M. All authors have read and agreed to the published version of the manuscript.

Funding: The authors appreciate the funding sources provided by the Tecnológico Nacional de México (TecNM) through the grant numbers 15455.22-P and 13559.22-P. The article processing charge was funded by Tecnologico de Monterrey.

Institutional Review Board Statement: Not applicable.

Informed Consent Statement: Not applicable.

Data Availability Statement: Not applicable.

Conflicts of Interest: The authors declare no conflict of interest.

References

1. Rockström, J.; Steffen, W.; Noone, K.; Persson, Å.; Chapin, F.S.; Lambin, E.; Lenton, T.M.; Scheffer, M.; Folke, C.; Schellnhuber, H.J.; et al. Planetary boundaries: Exploring the safe operating space for humanity. *Ecol. Soc.* **2009**, *14*, 32. [CrossRef]
2. Zou, C.; Zhao, Q.; Zhang, G.; Xiong, B. Energy revolution: From a fossil energy era to a new energy era. *Nat. Gas Ind. B* **2016**, *3*, 1–11. [CrossRef]
3. Wang, S.; Li, G.; Fang, C. Urbanization, economic growth, energy consumption, and CO_2 emissions: Empirical evidence from countries with different income levels. *Renew. Sustain. Energy Rev.* **2018**, *81*, 2144–2159. [CrossRef]
4. Intergovernmental Panel on Climate Change. *Climate Change 2014 Mitigation of Climate Change*; Intergovernmental Panel on Climate Change: Geneva, Switzerland, 2014.
5. Maamoun, N. The Kyoto protocol: Empirical evidence of a hidden success. *J. Environ. Econ. Manag.* **2019**, *95*, 227–256. [CrossRef]
6. Pastero, L.; Curetti, N.; Ortenzi, M.A.; Schiavoni, M.; Destefanis, E.; Pavese, A. CO_2 capture and sequestration in stable Ca-oxalate, via Ca-ascorbate promoted green reaction. *Sci. Total Environ.* **2019**, *666*, 1232–1244. [CrossRef]
7. Gao, W.; Liang, S.; Wang, R.; Jiang, Q.; Zhang, Y.; Zheng, Q.; Xie, B.; Toe, C.Y.; Zhu, X.; Wang, J.; et al. Industrial carbon dioxide capture and utilization: State of the art and future challenges. *Chem. Soc. Rev.* **2020**, *49*, 8584–8686. [CrossRef]
8. Xiao, X.; Xu, Y.; Lv, X.; Xie, J.; Liu, J.; Yu, C. Electrochemical CO_2 reduction on copper nanoparticles-dispersed carbon aerogels. *J. Colloid Interface Sci.* **2019**, *545*, 1–7. [CrossRef]
9. Sirijaraensre, J.; Limtrakul, J. Hydrogenation of CO_2 to formic acid over a Cu-embedded graphene: A DFT study. *Appl. Surf. Sci.* **2016**, *364*, 241–248. [CrossRef]
10. Alper, E.; Orhan, O.Y. CO_2 utilization: Developments in conversion processes. *Petroleum* **2017**, *3*, 109–126. [CrossRef]
11. Qiao, J.; Liu, Y.; Hong, F.; Zhang, J. A review of catalysts for the electroreduction of carbon dioxide to produce low-carbon fuels. *Chem. Soc. Rev.* **2014**, *43*, 631–675. [CrossRef]
12. Khan, I.; Saeed, K.; Khan, I. Nanoparticles: Properties, applications and toxicities. *Arab. J. Chem.* **2019**, *12*, 908–931. [CrossRef]
13. Duan, Y.-X.; Meng, F.-L.; Liu, K.-H.; Yi, S.-S.; Li, S.-J.; Yan, J.-M.; Jiang, Q. Amorphizing of Cu Nanoparticles toward Highly Efficient and Robust Electrocatalyst for CO_2 Reduction to Liquid Fuels with High Faradaic Efficiencies. *Adv. Mater.* **2018**, *30*, e1706194. [CrossRef] [PubMed]
14. Li, Z.; He, D.; Yan, X.; Dai, S.; Younan, S.; Ke, Z.; Pan, X.; Xiao, X.; Wu, H.; Gu, J. Size-Dependent Nickel-Based Electrocatalysts for Selective CO_2 Reduction. *Angew. Chemie* **2020**, *132*, 18731–18736. [CrossRef]
15. Riani, P.; Garbarino, G.; Cavattoni, T.; Canepa, F.; Busca, G. Unsupported cobalt nanoparticles as catalysts: Effect of preparation method on catalytic activity in CO_2 methanation and ethanol steam reforming. *Int. J. Hydrogen Energy* **2019**, *44*, 27319–27328. [CrossRef]
16. Naito, M.; Yokoyama, T.; Hosokawa, K.; Nogi, K. *Nanoparticle Technology Handbook*; Elsevier: Amsterdam, The Netherlands, 2018. ISBN 9780444641106.
17. Gosens, I.; Post, J.A.; De La Fonteyne, L.J.J.; Jansen, E.H.J.M.; Geus, J.W.; Cassee, F.R.; De Jong, W.H. Impact of agglomeration state of nano- and submicron sized gold particles on pulmonary inflammation. *Part. Fibre Toxicol.* **2010**, *7*, 37. [CrossRef]
18. Zare, Y.; Rhee, K.Y.; Hui, D. Influences of nanoparticles aggregation/agglomeration on the interfacial/interphase and tensile properties of nanocomposites. *Compos. Part B Eng.* **2017**, *122*, 41–46. [CrossRef]
19. Ghosh, S.K.; Calizo, I.; Teweldebrhan, D.; Pokatilov, E.P.; Nika, D.L.; Balandin, A.A.; Bao, W.; Miao, F.; Lau, C.N. Extremely high thermal conductivity of graphene: Prospects for thermal management applications in nanoelectronic circuits. *Appl. Phys. Lett.* **2008**, *92*, 151911. [CrossRef]
20. Sur, U.K. Graphene: A Rising Star on the Horizon of Materials Science. *Int. J. Electrochem.* **2012**, *2012*, 237689. [CrossRef]
21. Cruz-Martínez, H.; Rojas-Chávez, H.; Montejo-Alvaro, F.; Peña-Castañeda, Y.; Matadamas-Ortiz, P.; Medina, D. Recent Developments in Graphene-Based Toxic Gas Sensors: A Theoretical Overview. *Sensors* **2021**, *21*, 1992. [CrossRef]
22. Mali, K.S.; Greenwood, J.; Adisoejoso, J.; Phillipson, R.; De Feyter, S. Nanostructuring graphene for controlled and reproducible functionalization. *Nanoscale* **2015**, *7*, 1566–1585. [CrossRef]
23. Sánchez-Rodríguez, E.; Vargas-Hernández, C.; Cruz-Martínez, H.; Medina, D. Stability, magnetic, energetic, and reactivity properties of icosahedral $M@Pd_{12}$ (M = Fe, Co, Ni, and Cu) core-shell nanoparticles supported on pyridinic N_3-doped graphene. *Solid State Sci.* **2020**, *112*, 106483. [CrossRef]
24. Wang, Q.; Tian, Y.; Chen, G.; Zhao, J. Theoretical insights into the energetics and electronic properties of MPt_{12} (M = Fe, Co, Ni, Cu, and Pd) nanoparticles supported by N-doped defective graphene. *Appl. Surf. Sci.* **2017**, *397*, 199–205. [CrossRef]
25. Montejo-Alvaro, F.; González-Quijano, D.; Valmont-Pineda, J.A.; Rojas-Chávez, H.; Juárez-García, J.M.; Medina, D.I.; Cruz-Martínez, H. CO_2 Adsorption on PtCu Sub-Nanoclusters Deposited on Pyridinic N-Doped Graphene: A DFT Investigation. *Materials* **2021**, *14*, 7619. [CrossRef] [PubMed]
26. Dongare, S.; Singh, N.; Bhunia, H. Nitrogen-doped graphene supported copper nanoparticles for electrochemical reduction of CO_2. *J. CO_2 Util.* **2020**, *44*, 101382. [CrossRef]

27. Wang, M.; Zhang, B.; Ding, J.; Xu, N.; Bernards, M.T.; He, Y.; Shi, Y. Three-Dimensional Nitrogen-Doped Graphene Aerogel-Supported MnO Nanoparticles as Efficient Electrocatalysts for CO_2 Reduction to CO. *ACS Sustain. Chem. Eng.* **2020**, *8*, 4983–4994. [CrossRef]
28. Wang, H.; Nie, X.; Guo, X.; Song, C. A computational study of adsorption and activation of CO_2 and H_2 over Fe(1 0 0) surface. *J. CO_2 Util.* **2016**, *15*, 107–114. [CrossRef]
29. Dean, J.; Yang, Y.; Austin, N.; Veser, G.; Mpourmpakis, G. Design of Copper-Based Bimetallic Nanoparticles for Carbon Dioxide Adsorption and Activation. *ChemSusChem* **2018**, *11*, 1169–1178. [CrossRef]
30. Ocampo-Restrepo, V.K.; Zibordi-Besse, L.; Da Silva, J.L.F. Ab initio investigation of the atomistic descriptors in the activation of small molecules on 3*d* transition-metal 13-atom clusters: The example of H_2, CO, H_2O, and CO_2. *J. Chem. Phys.* **2019**, *151*, 214301. [CrossRef]
31. Pangh, A. Catalytic cleavage of CO_2 on bimetallic Ni_4M (M = Ni, Mo, Sc, and Y) nanoclusters: A DFT study. *Catal. Commun.* **2020**, *149*, 106245. [CrossRef]
32. Austin, N.; Butina, B.; Mpourmpakis, G. CO_2 activation on bimetallic CuNi nanoparticles. *Prog. Nat. Sci.* **2016**, *26*, 487–492. [CrossRef]
33. Geudtner, G.; Calaminici, P.; Carmona-Espíndola, J.; del Campo, J.M.; Domínguez-Soria, V.D.; Moreno, R.F.; Gamboa, G.U.; Goursot, A.; Köster, A.M.; Reveles, J.U.; et al. deMon2k. *Wiley Interdiscip. Rev. Comput. Mol. Sci.* **2012**, *2*, 548–555. [CrossRef]
34. Zhang, Y.; Yang, W. Comment on "Generalized Gradient Approximation Made Simple". *Phys. Rev. Lett.* **1998**, *80*, 890. [CrossRef]
35. Calaminici, P.; Janetzko, F.; Köster, A.M.; Mejia-Olvera, R.; Zuniga-Gutierrez, B. Density functional theory optimized basis sets for gradient corrected functionals: 3*d* transition metal systems. *J. Chem. Phys.* **2007**, *126*, 044108. [CrossRef]
36. Neese, F. Software update: The ORCA program system, version 4.0. *Wiley Interdiscip. Rev. Comput. Mol. Sci.* **2018**, *8*, 1–6. [CrossRef]
37. Weigend, F.; Ahlrichs, R. Balanced basis sets of split valence, triple zeta valence and quadruple zeta valence quality for H to Rn: Design and assessment of accuracy. *Phys. Chem. Chem. Phys.* **2005**, *7*, 3297–3305. [CrossRef]
38. Boys, S.F.; Bernardi, F.D. The Calculation of small molecular interactions by the differences of separate total energies. Some procedures with reduced errors. *Mol. Phys.* **1970**, *19*, 553–566. [CrossRef]
39. Grimme, S.; Ehrlich, S.; Goerigk, L. Effect of the damping function in dispersion corrected density functional theory. *J. Comput. Chem.* **2011**, *32*, 1456. [CrossRef]
40. Lu, T.; Chen, F. Multiwfn: A multifunctional wavefunction analyzer. *J. Comput. Chem.* **2012**, *33*, 580–592. [CrossRef]
41. Wang, Y.; Wang, L.; Ma, S. Role of defects in tuning the adsorption of CO over graphene-supported Co13 cluster. *Appl. Surf. Sci.* **2019**, *481*, 1080–1088. [CrossRef]
42. Montejo-Alvaro, F.; Rojas-Chávez, H.; Herrera-Rivera, R.; Mtz-Enriquez, A.; Cruz-Martínez, H.; Medina, D. Investigating the stability of icosahedral $Ni_{13-x}Cu_x$ (x = 1–12) bimetallic nanoclusters supported on defective graphene: Insights from first-principles calculations. *Phys. E Low-dimensional Syst. Nanostructures* **2019**, *118*, 113880. [CrossRef]
43. Liu, L.; Su, Y.; Gao, J.; Zhao, J. Electronic and magnetic properties for Co_{13} clusters deposited on graphene: A first-principles exploration. *Phys. E Low-dimensional Syst. Nanostructures* **2012**, *46*, 6–11. [CrossRef]
44. Alonso-Lanza, T.; Ayuela, A.; Aguilera-Granja, F. Chemical Bonding of Transition-Metal Co_{13}Clusters with Graphene. *ChemPhysChem* **2015**, *16*, 3700–3710. [CrossRef]
45. Montejo-Alvaro, F.; Oliva, J.; Zarate, A.; Herrera-Trejo, M.; Hdz-García, H.; Mtz-Enriquez, A. Icosahedral transition metal clusters (M_{13}, M = Fe, Ni, and Cu) adsorbed on graphene quantum dots, a DFT study. *Phys. E Low-dimensional Syst. Nanostructures* **2019**, *110*, 52–58. [CrossRef]
46. García-Rodríguez, D.; Mendoza-Huizar, L.; Díaz, C. A DFT study of Cu nanoparticles adsorbed on defective graphene. *Appl. Surf. Sci.* **2017**, *412*, 146–151. [CrossRef]
47. Ruiz-Morales, Y. HOMO-LUMO gap as an index of molecular size and structure for polycyclic aromatic hydrocarbons (PAHs) and asphaltenes: A theoretical study. I. *J. Phys. Chem. A* **2002**, *106*, 11283–11308. [CrossRef]
48. Caglar, A.; Düzenli, D.; Onal, I.; Tezsevin, I.; Sahin, O.; Kivrak, H. A novel experimental and density functional theory study on palladium and nitrogen doped few layer graphene surface towards glucose adsorption and electrooxidation. *J. Phys. Chem. Solids* **2020**, *150*, 109684. [CrossRef]
49. Mendes, P.C.D.; Ocampo-Restrepo, V.K.; Da Silva, J.L.F. Ab initio investigation of quantum size effects on the adsorption of CO_2, CO, H_2O, and H_2 on transition-metal particles. *Phys. Chem. Chem. Phys.* **2020**, *22*, 8998–9008. [CrossRef]